Magnetic anisotropy and slow relaxation of magnetisation in double salts containing four- and six-coordinate cobalt(II) complex ions†

Jana Juráková, [a,b] Vinicius Tadeu Santana, [a] Ján Pavlik, [b] Ján Moncoľ, [b] Ivan Nemec,[a,c] Miguel Clemente-León, [d] Senthil Kumar Kuppusamy, [e] Mario Ruben,[e] Erik Čižmár [f] and Ivan Šalitroš *[a,b]

Four novel Co(II) coordination compounds **1–4** of the general formula $[Co(L^n)_2][Co(NCY)_4]\cdot m CH_3CN$ (where L^n are tridentate ligands L1 = 2,6-bis(1-hexyl-1*H*-benzimidazol-2-yl)pyridine for **1** and **2**; L2 = 2,6-bis(1-octyl-1*H*-benzimidazol-2-yl)pyridine for **3**; L3 = 2,6-bis(1-dodecyl-1*H*-benzimidazol-2-yl)pyridine for **4**, Y = O for **1**, **3**, and **4** and Y = S for **2**; m = 0 for **1** and **3**, m = 0.5 for **2** and m = 2 for **4**) were prepared and characterised. The molecular structures of all four compounds consist of the hexacoordinate complex cation $[Co(L^n)_2]^{2+}$ and tetracoordinate complex anion $[Co(NCY)_4]^{2-}$, with distorted octahedral and tetrahedral symmetry of coordination polyhedra, respectively. The electronic structures of all compounds feature an orbitally non-degenerate ground state well-separated from the lowest excited state, which allows the analysis of the magnetic anisotropy by the spin Hamiltonian model. ZFS parameters, derived from both CASSCF-NEVPT2 calculations and magnetic data analysis, indicate that tetrahedral anions $[Co(NCY)_4]^{2-}$ exhibit small axial parameters $|D|$ spanning the range of 2.2 to 7.7 cm^{-1}, while octahedral cations $[Co(L^n)_2]^{2+}$ display significantly larger $|D|$ parameters in the range of 37 to 95 cm^{-1}. For **1–3**, the Fourier-transform infrared magnetic spectroscopy (FIRMS) revealed a reasonable transmission with a magnetic absorption around the expected value for the ZFS accompanied by features allowing to identify phonon frequencies and simulate spin-phonon couplings. Dynamic magnetic investigations unveiled the field-induced slow relaxation of magnetisation, with maximal relaxation times (τ) of 92(2) μs for **2** at 2 K and B_{DC} = 0.3 T. The temperature evolution of τ was analysed using a combination of Orbach, direct and Raman relaxations (U_{eff} = 8(1) K (5.6 cm^{-1})) or Orbach, direct and spin-phonon induced relaxations (U_{eff} = 10.3(9) K (7.2 cm^{-1})). The rest of the complexes, namely **1**, **3**, and **4** show field-induced slow relaxation of magnetisation with τ smaller than 16 μs.

Introduction

Over the past three decades, significant progress has been witnessed in the realm of single-molecule magnets (SMMs), characterized by their captivating magnetic properties such as magnetic hysteresis and the slow relaxation of magnetization (SRM) at the molecular scale.[1] The importance of these molecules stems from their potential uses in molecular spintronic,[2] qubit[3] and data storage[4] nanotechnology. Magnetic bistability, defined by the existence of two opposite projections of magnetisation within the hysteresis loop, is associated with the presence of the energy barrier for spin reversal (U). In 3d-metal complexes, U is commonly related to the zero-field splitting (ZFS) of the ground spin state, formulated as $U = |D|S^2$ for an even number of unpaired electrons, and $U = |D|(S^2 - 1/4)$ for an odd number of unpaired electrons in the metal ion's valence shell. Here, D represents the axial ZFS parameter outlined in the spin

[a]*Central European Institute of Technology, Brno University of Technology, Purkyňova 123, 61200 Brno, Czech Republic*

[b]*Department of Inorganic Chemistry, Faculty of Chemical and Food Technology, Slovak University of Technology in Bratislava, Bratislava SK-81237, Slovakia. E-mail: ivan.salitros@stuba.sk*

[c]*Department of Inorganic Chemistry, Faculty of Science, Palacký University, 17. listopadu 12, 771 46 Olomouc, Czech Republic*

[d]*Instituto de Ciencia Molecular (ICMol), Universidad de Valencia, Catedrático José Beltrán 2, 46980 Paterna, Spain*

[e]*Institute of Nanotechnology (INT), Karlsruhe Institute of Technology (KIT), Hermann-von-Helmholtz-Platz 1, 76344 Eggenstein-Leopoldshafen, Germany*

[f]*Institute of Physics, Faculty of Science, P.J. Šafárik University, Park Angelinum 9, 04154 Košice, Slovakia*

Hamiltonian formalism. Therefore, an intriguing aspect of SMMs involves the fine-tuning of magnetic anisotropy through modulation of the ligand field strength and coordination geometry surrounding the central atom. Considerable attention has been focused on Co(II) coordination compounds as promising avenues for the development of novel and stable SMMs.[5] This preference arises from their robust magnetic anisotropies, which exhibit both easy-axis and easy-plane characteristics, as indicated by negative and positive ZFS splitting parameters D, respectively.[6] Consequently, these properties lead to the observation of SRM, irrespective of the sign of the D values. Indeed, the phenomenon of SRM has been observed in various Co(II) complexes with different coordinate geometries and coordination numbers, ranging from two to eight.[5]

Among the various families of Co(II)-SMMs, Co(II) complexes with 2,6-bis(benzimidazole-1-yl)pyridine (bbp) tridentate ligands present a well-established category of field-induced SMMs.[5b] The rigid and aromatic nature of these ligands favours the ligand field strength that promotes higher magnetic anisotropy, thus resulting in a significant axial ZFS parameter. The ligand field strength can be tuned by the rationalised introduction of substituents onto the ligand skeleton having the impact on the relaxation of magnetisation, which can occur through either single or multiple relaxation channels. Furthermore, the goal-directed functionalisation of bbp ligands has an impact also on the other physicochemical properties like solubility, polarity or thermal stability. For instance, our recent studies have specifically focused on mononuclear Co(II)-SMMs utilizing bbp ligands functionalized with long aliphatic chains exhibiting pronounced solubility in non-polar and volatile solvents typically used for lithographical depositions.[7]

The coordination chemistry of the Co(II)-bbp system presents a range of possibilities for coordination numbers and geometries, which in turn influence the crystal field strength and properties of the resulting Co(II)-SMMs. When monodentate X (such as halide or pseudohalide anions) or two-donor ligands A (nitrates or carboxylates) are involved in the complex synthesis, the formation of pentacoordinate [Co(bpp)X_2],[7a,b,8] hexacoordinate [Co(bbp)(κ_1-A)(κ_2-A)][7c] or potentially heptacoordinate [Co(bbp)(κ_2-A)$_2$] complexes can be observed. Apart from the neutral complexes, the hexacoordinate [Co(bbp)$_2$]$^{2+}$ complex cations can be prepared as well and isolated in the form of complex salts. Another possibility is the formation of coordination compounds containing both octahedral cationic and tetrahedral anionic moieties, represented by the general formula [Co(bbp)$_2$][CoX_4].[9] These compounds serve as pseudoisomers to [Co(bpp)X_2], as they share the same empirical formulae, and it is currently unclear which reaction conditions favour the formation of ionic compounds [Co(bbp)$_2$][CoX_4] over pentacoordinate neutral complexes. In 2017, Konar and co-workers reported the complexation of *in situ* prepared Co(NCS)$_2$ with bbp in methanol–water solution affording the precipitate of [Co(bpp)(NCS)$_2$], while the remaining brown mother liquor was not analysed further. A few years after, Mondal and co-workers reported the same synthesis performed in methanol–dichloromethane solution, which offered a green precipitate of [Co(bbp)$_2$][Co(NCS)$_4$] and pink mother liquor of [Co(bpp)(NCS)$_2$]. Furthermore, literature survey allowed us to recognise a handful of similar coordination compounds [Co(L)$_2$][Co(X_{ps})$_4$] with hexacoordinated complex cations containing the tridentate aromatic N-donor ligands L and tetrahedral complex anions with pseudohalido ligands X_{ps} (Table S1†). These reports document the complexation of Co(II) pseudohalide salts with tridentate ligands L in common solvents such as methanol, acetonitrile, and chloroform consistently resulting in the exclusive formation of [Co(L)$_2$][Co(X_{ps})$_4$] ionic coordination compounds, irrespective of temperature, reaction duration, or crystallization conditions.[10] Thus apparently, the conditions and factors governing the formation of related pseudoisomers [Co(L)(X_{ps})$_2$] and [Co(L)$_2$][Co(X_{ps})$_4$] remain unexplained.

Herein we report on four coordination compounds of the general formula [Co(L^n)$_2$][Co(NCY)$_4$]·mCH$_3$CN (where L^n are tridentate ligands L1 = 2,6-bis(1-hexyl-1*H*-benzimidazol-2-yl)pyridine for **1** and **2**; L2 = 2,6-bis(1-octyl-1*H*-benzimidazol-2-yl)pyridine for **3**; L3 = 2,6-bis(1-dodecyl-1*H*-benzimidazol-2-yl)pyridine for **4**, Y = O for **1**, **3**, and **4** and Y = S for **2**; m = 0 for **1** and **3**, m = 0.5 for **2** and m = 2 for **4**). All compounds were prepared by straightforward complexation of Co(NCY)$_2$ salts with the corresponding bbp derivatives L1–L3 in acetonitrile solution. The prepared compounds were structurally characterised and their static and dynamic magnetic properties were investigated in detail.

Synthesis and spectral and structural properties

The detailed synthetic procedures and characterisation of the reported compounds **1–4** are described in the Experimental section (see the ESI†). All four coordination compounds were synthesized by the complexation of Co(NCO)$_2$ or Co(NCS)$_2$ with the corresponding bbp derivative L^n (L1 for **1** and **2**, L2 for **3** and L3 for **4**) in acetonitrile at elevated temperature. The reactions yielded green block crystals suitable for single-crystal X-ray analysis after a few days of slow evaporation at room temperature. The phase purity of the prepared materials was confirmed by powder X-ray diffraction analysis (Fig. S3†), demonstrating that the employed synthetic procedure yields ionic compounds [Co(L^n)$_2$][Co(NCY)$_4$]·mCH$_3$CN, rather than neutral complexes [Co(L^n)(NCY)$_2$].

As the molecular structures of complexes **1–4** differ only in the length of aliphatic chains and pseudohalide ligand anions, their FT-IR (Fig. S4†) and UV-vis (Fig. S5†) spectra are similar. The stretching vibrations of aliphatic C–H bonds were observed in the intervals of 2925–2922 cm^{-1} and 2854–2851 cm^{-1} for asymmetric and symmetric valence vibrations, respectively. Medium vibrational bands corresponding to aromatic C–C or C–N stretching were recorded in the range of 1598–1566 cm^{-1}. Vibrations of C≡N bonds in the cyanate ligand anion are observed within the range of 2207–2190 cm^{-1}, the C≡N vibration of the thiocyanate ligand

anion in compound **2** is shifted to lower frequencies, specifically at 2099 cm ^{1}. The solution UV-VIS absorption spectra of **1–4** revealed a broad band in the interval 270–420 nm split to two maxima centred at 313 nm and 343 nm, which corres-ponds to intra-ligand $\pi \rightarrow \pi^*$ and $n \rightarrow \pi^*$ transitions, respectively.

Compounds **1–4** possess similar molecular structures (Fig. 1) consisting of an hexacoordinate complex cation $[Co(L^n)_2]^{2+}$ and a tetracoordinate complex anion $[Co(NCY)_4]^{2}$ (where Y = O for **1**, **3**, **4** and Y = S for **2**). Single crystal X-ray diffraction analysis revealed the triclinic $P\bar{1}$ space group for compounds **1** (at 293 K), **2** (at 100 K) and **3** (at 293 K), and monoclinic $P2_1/c$ space group for **4** (at 100 K). Selected crystallographic information is listed in Table S2.† The crystal structure of **2** comprises two formula units $[Co(L1)_2][Co(NCS)_4]\cdot 0.5CH_3CN$ within its asymmetric unit. In contrast, the asym-

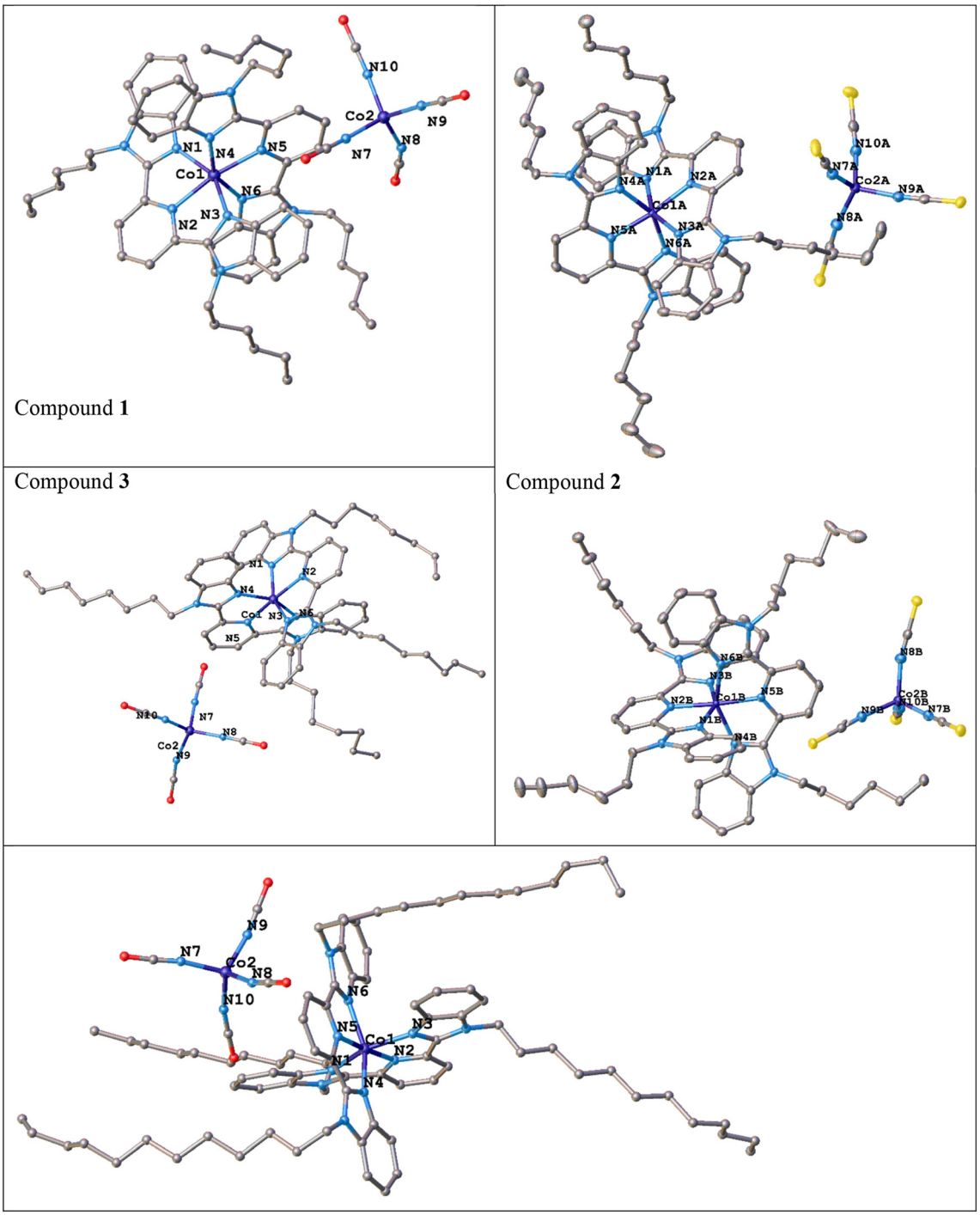

Fig. 1 Molecular structures of the reported compounds (hydrogen atoms and lattice solvent molecules are omitted).

metric unit of the remaining structures **1**, **3** and **4** contain a single formula unit $[Co(L1)_2][Co(NCO)_4]$, $[Co(L2)_2][Co(NCO)_4]$ and $[Co(L3)_2][Co(NCO)_4]\cdot 2CH_3CN$, respectively. The hexacoordinate complex cations $[Co(L^n)_2]^{2+}$ in compounds **1–4** exhibit a distorted octahedral geometry, characterized by *cis* N–Co–N angle ranges of 75.3–114.1° for **1**, 75.3–110.3° for **2**, 75.5–112.5° for **3**, and 75.9–107.6° for **4**. This angular octahedral distortion is further quantified by metric distortion parameters Σ[11] and symmetry measure parameters S(OC),[12] as determined by SHAPE analysis (Table S4†). Calculated values within the ranges of 124°–137° for Σ and 4.0–4.9 for S(OC-6) clearly indicate significant deviation from ideal octahedral symmetry. The Co–N bond distances exhibit a slight dependence on the nature of the nitrogen donor atom. Co–N bonds involving pyridine N-donor atoms range from 2.088 Å to 2.117 Å, slightly shorter than Co–N bonds containing imidazole N-donor atoms, which range from 2.110 Å to 2.162 Å (Table S3†).

The coordination polyhedra of $[Co(NCY)_4]^{2-}$ complex anions in **1–4** adopt a tetrahedral geometry. The N–Co–N angles vary between 105.8° and 113.5°, with an average Co–N bond length of 1.96 Å. The deviation from tetrahedral symmetry has been evaluated using the distortion parameter τ_4 and SHAPE analysis. Complex anions in **1**, **3** and **4** exhibit only negligible angular deviation from tetrahedral angles (Table S4†) and therefore the metric parameters acquire the values $\tau_4 \approx 1$ and S(T-4) ≈ 0, typical of an almost ideal tetrahedron. However, $[Co(NCS)_4]^{2-}$ complex anions of compound **2** show the most pronounced deviation from the tetrahedral shape among the reported compounds, with the metric parameters τ_4 = 0.94(Co2A) and 0.89 (Co2B), S(T-4) ≈ 0.2 (Co2A) and 0.5 (Co2B).

Static magnetic investigation and computational study

Temperature and field dependent measurements of magnetization were performed in the temperature range 2–300 K at a static magnetic field B_{DC} = 0.1 T and at constant temperatures in the field range B_{DC} = 0–7 T. Both measurements are presented in Fig. 2 as χT *vs.* T and M_{mol} *vs.* B functions. The room temperature values of χT (4.90–5.77 $cm^3\ mol^{-1}\ K^{-1}$) are significantly higher than the spin-only value for the S = 3 system (S = 2 × 3/2, g = 2.0; χT = 2 × 1.875 $cm^3\ mol^{-1}\ K^{-1}$) suggesting considerable contribution of angular momentum. As the temperature decreases, the χT product gradually decreases, and below 50 K, the decrease becomes abrupt, reaching 3.32 $cm^3\ mol^{-1}\ K^{-1}$ for **1**, 3.87 $cm^3\ mol^{-1}\ K^{-1}$ for **2**, 2.94 $cm^3\ mol^{-1}\ K^{-1}$ for **3** and 3.49 $cm^3\ mol^{-1}\ K^{-1}$ for **4** at 2 K. Molar magnetization M_{mol} at 7 T and 2 K acquires lower values (4.62–5.39μ_B) than that expected for a Curie paramagnet with S = 3 (6μ_B), which indicates notable magnetic anisotropy. All studied systems **1–4** are formed by two different Co(II) sites in their molecular structure – an octahedral one and a tetrahedral one. While there is no firm justification for the contribution of orbital angular momentum in the tetrahedrally coordinated Co(II) centres, its presence in the octahedral centres depends strongly upon subtle geometry changes of the coordination environment.[13] Therefore an *ab initio* study was performed on the simplified model systems **Ioct–IVoct** (Fig. S6†). It turned out that in all four cases the first excited spin-quartet state is distant enough from the ground spin-quartet state (as a rule of thumb more than 1000 cm^{-1}, see Fig. S7†) meaning that the effect of angular momentum can be projected on the g-tensor components in the Spin Hamiltonian formalism. The following convention of the Hamiltonian has been used

$$\hat{H}_{SH} = D_{oct}\hat{S}_{z,oct}^{\ 2} + E_{oct}(\hat{S}_{x,oct}^{\ 2} - \hat{S}_{y,oct}^{\ 2}) + \mu_B B \sum_{a=x,y,z} (\hat{S}_{a,oct} \cdot g_{a,oct}) + D_{tetr}\hat{S}_{z,tetr}^{\ 2} + \mu_B B g_{avg,tetr} \sum_{a=x,y,z} \hat{S}_{a,tetr} \quad (1)$$

where D_i is the axial parameter of zero-field splitting (ZFS), E_{oct} is the rhombic ZFS parameter and g-parameters were considered spatially resolved for the octahedral case (*i.e.* $g_{x,oct}$, $g_{y,oct}$ and $g_{z,oct}$) while for the tetrahedral case an isotropic averaged parameter $g_{avg,tetr}$ was considered. To reproduce experimental magnetic functions, the molecular field quantified by parameter zJ (Fig. S8 and Table S5†) and temperature-independent magnetism had to be included, too. The calculated values of parameters obtained from *ab initio* calculations are collected in Table 1, the optimum parameter values from simultaneous fitting of the experimental curves χT *vs.* T and M_{mol} *vs.* B are collected in Table 2 and the fitted curves are displayed in Fig. 2. In all cases a good mutual agreement can be noted. The experimental D values for the octahedral sites range widely from +49 to +95 cm^{-1} and do not correlate with the angular distortion of the corresponding coordination polyhedra (Table S4†). On the other hand, the small positive or negative D values for the tetrahedral sites are similar to those already reported for complex salts containing $[Co(NCY)_4]^{2-}$ anions.[14]

The experimental curves are compared with the optimum fit ones and predicted ones in Fig. 2. One can see that except for the case of system **1**, the spin Hamiltonian model was able to describe excellently both independent data sets. The agreement of theoretically predicted curves with experimental results is, however, generally worse. Since the *ab initio* approach did not consider possible weak exchange interactions between the centres (*i.e.* molecular field), such a discrepancy is justified for the thermal behaviour of χT. In the case of magnetization, the higher saturation values of magnetization correlate with significantly lower values of axial anisotropy parameters predicted for **Ioct** and **IIIoct**.[1,6]

Fourier-transform infrared magneto spectroscopy

Fourier-transform infrared magneto spectroscopy (FIRMS) makes possible the experimental observation of the zero-field splitting $\Delta = \sqrt{D^2 + 3E^2}$ between the ground and excited

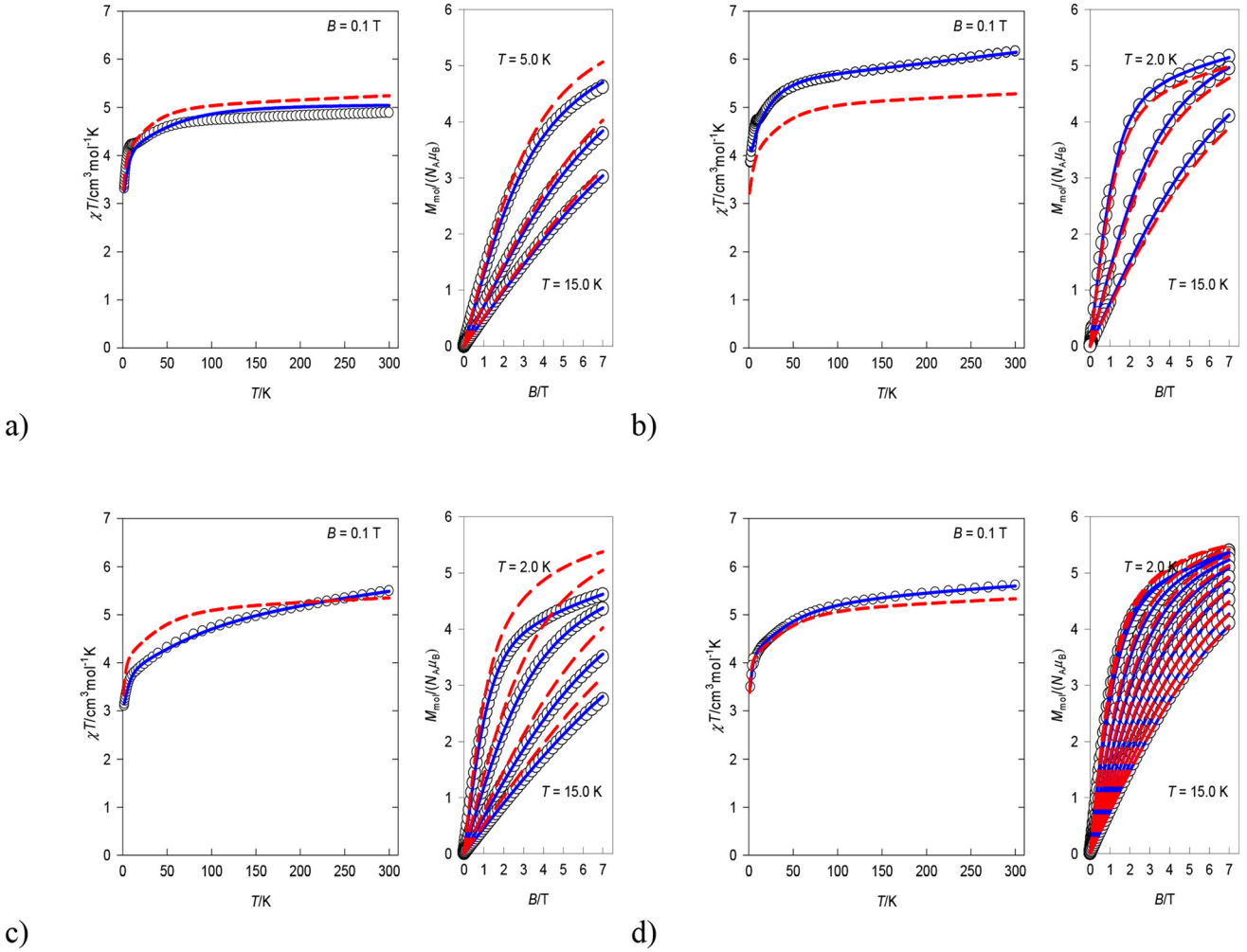

Fig. 2 Magnetic functions analysed by the Spin Hamiltonian formalism for (a) compound **1**; (b) compound **2**; (c) compound **3** and (d) compound **4**. Left: susceptibility–temperature product with respect to temperature, right: magnetization per centre with respect to the magnetic field; empty circles: experiment, blue solid line: optimum fit, and red dashed line: *ab initio* prediction based on model molecules.

Table 1 Calculated values of ZFS parameters for respective Co(II) centres obtained by *ab initio* calculations (cm^{-1})

	Ioct	Itetr	IIoct	IItetr	IIIoct	IIItetr	IVoct	IVtetr
D	40.8	−3.2	52.0 (47.0)[a]	6.0	57.1	−3.5	57.7	2.2
E/D	0.11	0.14	0.06	0.20	0.04	0.08	0.01	0.29
g_z	2.06	2.23	2.02	2.19	2.01	2.23	2.00	2.23
g_x	2.40	2.24	2.46	2.26	2.49	2.23	2.50	2.25
g_y	2.53	2.27	2.53	2.28	2.57	2.27	2.52	2.27

[a] The simulation of the data obtained by FIRMS used all the same parameters from this table, except for the D value of compound **2**, displayed in brackets here.

doublets for $S = 3/2$ systems.[7b,15] The determination of D and E separately as well as the sign of D requires a combination of FIRMS with high-frequency electron paramagnetic resonance (HFEPR) results.[7b,15g] However, HFEPR was complicated by the presence of the two Co(II) sites in the studied compounds. Therefore, we performed only FIRMS at 4.2 K from 0 T to 16 T and combined the spin Hamiltonian parameters obtained from *ab initio* and magnetization results to conduct our analysis. Experimental details are found in the ESI.† Compounds **1–3** displayed reasonable transmission with a magnetic absorption around the expected value for the ZFS according to *ab initio* calculation values from Table 1, including anti-crossing features, which are typical signatures of spin–phonon coupling.[16] Compound **4** did not show any magnetic absorption despite the pellet having a reasonable transmission. We attribute the lower intensity of the magnetic absorption for **1**

Table 2 Optimum values of ZFS parameters for respective Co(II) centres obtained from experimental data (cm^{-1})

	1oct	1tetr	2oct	2tetr	3oct	3tetr	4oct	4tetr
D	70.0	−6.6	36.8	7.7	94.5	−7.5	49.2	3.8
g_z	2.00	2.40[a]	2.00	2.28[a]	2.00	2.20[a]	2.04	2.40[a]
g_x	2.20	2.40[a]	2.70	2.28[a]	2.54	2.20[a]	2.46	2.40[a]
g_y	2.51	2.40[a]	2.70	2.28[a]	2.60	2.20[a]	2.60	2.40[a]
zJ (10^{-3} cm^{-1})	−0.21		17.44		3.94		−0.56	
χ_{TIP} (10^{-3} cm^3 mol^{-1})	0.00		2.41		2.16		1.04	
R	0.233		0.068		0.003		0.008	

[a] In the case of tetrahedral systems all three components of the g-tensor were fixed at the same value.

and the absence of it for **4** to broadened magnetic peaks for those samples, indicating shorter relaxation times, especially compared to those of **2** and **3**. As the sensitivity is dependent on the linewidth, a broadened signal possesses a lower signal-to-noise ratio. Also, as the linewidth in magnetic resonance is inversely proportional to the relaxation time,[17] a broader signal corresponds to faster relaxation. This is confirmed by the dynamic magnetic investigation shown in the next section.

FIRMS colormaps (Fig. 3) were compared with the simulation of the octahedral sites of eqn (1) using the g matrix, D values and the rhombicity E/D obtained from *ab initio* calculations in Table 1 and the vibronic model described in the ESI Note 3† by Moseley *et al.*[16] to extract the phonon frequencies and the spin–phonon couplings, shown in Table 3. The resulting simulations are shown as black lines in Fig. 3, showing very good agreement of the positions of the magnetic peaks in the spectra with the simulation using the theoretically predicted spin Hamiltonian parameters. Not all simulated lines have a corresponding peak in the experimental data because the probability of transitions was not considered. Only for compound **2** the value of D used for the simulation was slightly different from the predicted one and that is indicated in Table 1. In the simulation Nain *et al.* discuss the role of the spin–phonon coupling as a relevant pathway for magnetic relaxation in Co(II) SMMs.[18] Given that all three examined samples are field-induced SMMs (*vide infra*), it is reasonable to anticipate the

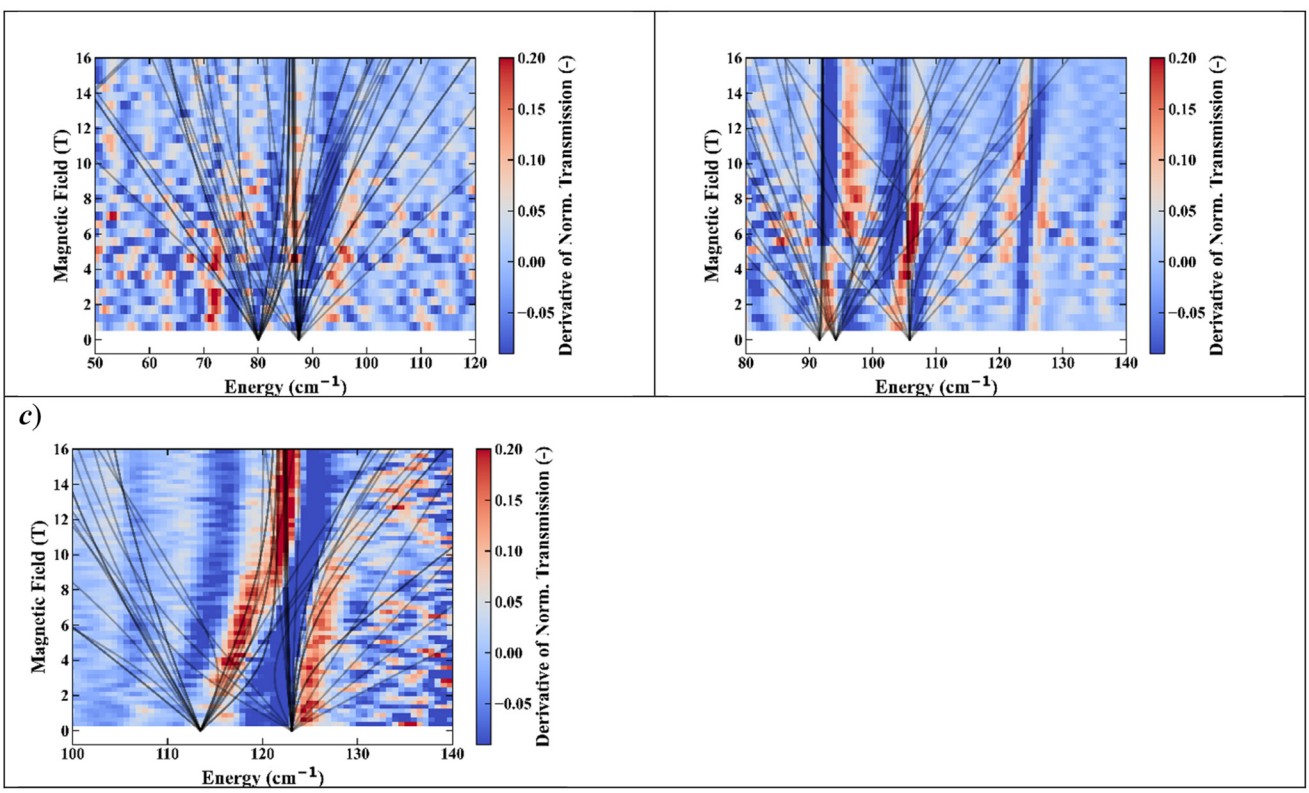

Fig. 3 Colormaps of the derivative of the normalized FIRMS transmission spectra for compounds (a) **1**, (b) **2** and (c) **3** measured at T = 4.2 K and a magnetic field of up to 16 T. The spectra were normalized by the average sum of all obtained spectra. The derivative aids the identification of the magnetic field-dependent features. The lines are simulated with the spin Hamiltonian and vibronic couplings with the parameters indicated in Tables 1 and 3.

Table 3 Values of the phonon modes $\hbar\omega_i$ and vibronic couplings e_i for respective Co(II) centers obtained by FIRMS (in cm^{-1})

	1oct	2oct	3oct
$\hbar\omega_1$	86	92	122
e_1	3	1	3
$\hbar\omega_2$	—	105	—
e_2	—	3	—
$\hbar\omega_3$	—	125	—
e_3	—	1	—

involvement of spin–phonon coupling in the SRM. Compounds **1–3** exhibit comparable vibronic coupling constants. However, compound **2** displays multiple vibronic couplings together with the longest magnetization relaxation, indicating the presence of another predominant relaxation pathway.

Dynamic magnetic investigation

The magnetic data induced by the oscillating alternating-current (AC) magnetic field were taken at an amplitude of B_{AC} = 0.5 mT and in the frequency range 10–10 000 Hz. At 2 K, no SRM was observed at B_{DC} = 0 T (Fig. S9–S13†), which is a consequence of the fast relaxation of magnetization resulting, for instance, from the quantum tunnelling effect induced by hyperfine interactions with the nuclear spins. However, the applied B_{DC} field suppressed the tunnelling, causing the emergence of the out-of-phase susceptibility component χ'', indicating that the reported compounds are field-induced SMMs. Based on the results of the B_{DC} field scan, three compounds (**1**, **3**, and **4**) do not show the maxima of χ'' susceptibility up to the highest measured frequency, which suggests that their relaxation times are faster than 16 μs. This is consistent with other similar ionic systems $[Co(L)_2][Co(X_{ps})_4]$ (Table S1†) which show very short relaxation times τ and the maxima of χ'' susceptibility located at very high frequencies. On the other hand, compound **2** does show the maxima of χ'' susceptibility above 1000 Hz, enabling a detailed investigation of SRM. The frequency dependent in-phase χ' and out-of-phase χ'' components of AC susceptibility were satisfactorily fitted to the extended one-set Debye model (eqn (S1) and (S2), see the ESI†), using which the isothermal χ_T and adiabatic χ_S susceptibilities along with the relaxation time τ and its distribution parameter α were determined at given static magnetic fields (Table S6 and Fig. S10†). The obtained τ *vs.* B dependence was successfully analysed with respect to the combination of direct and Raman relaxation mechanisms according to eqn (2) (Fig. 4a and Table 4).

$$\frac{1}{\tau} = AB^m T + d\left(\frac{1+eB^2}{1+fB^2}\right)T^n \qquad (2)$$

The AC susceptibility measurement of compound **3** in the DC field domain and at 2 K revealed a two-channel relaxation,

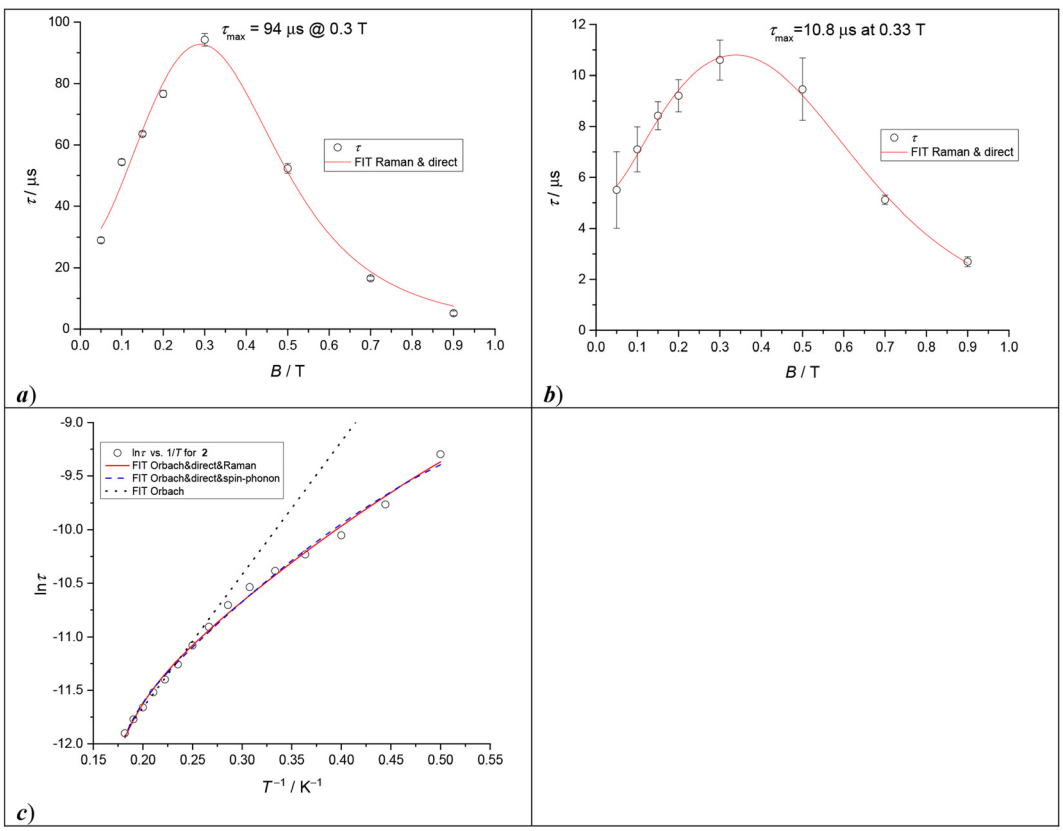

Fig. 4 τ *vs.* B dependence at T = 2 K for **2** (a) and **3** (b). ln τ *vs.* 1/T dependence at B_{DC} = 0.3 T for compound **2** (c).

with the maxima of both the low-frequency and high-frequency channels surpassing the hardware limits, below 10 Hz and above 10 kHz, respectively (Fig. S12†). However, the high onset of the latter relaxation channel allowed for its satisfactory analysis with respect to the two-set Debye model (eqn (S3), (S4) and Table S9†), while the parameters for the less pronounced low-frequency channel were ignored. The τ *vs.* B dependence with the maximum τ_{max} = 10.8 μs at 0.33 T was fitted to a combination of Raman and direct relaxation mechanisms (eqn (2) and Fig. 4b).

The temperature variable measurement of compound **2** (Fig. S11 and Table S7†) was carried out at a B_{DC} = 0.3 T field, where the τ acquires the highest value (92(2) μs at 2 K). The obtained $\ln\tau$ *vs.* $1/T$ dependence was analysed with respect to a combination of various relaxation mechanisms. At first, the effective energy barrier was estimated using linear fit in a high-temperature region (4.5–5.5 K), which resulted in U_{eff} = 12.4 K and $\tau_0 = 7.2 \times 10^{-7}$ s (Fig. 4c, dotted black curve). However, a comprehensive analysis of $\ln\tau$ *vs.* $1/T$ over the whole temperature range requires a combination of two or three relaxation processes according to eqn (3), with direct, Raman and Orbach terms, respectively.

$$\frac{1}{\tau} = aB^m T + CT^n + \frac{1}{\tau_0}\exp\left(-\frac{U_{eff}}{kT}\right) \quad (3)$$

Among several combinations of two or three relaxation processes (Table S7†), the most meaningful parameters along with the reasonable accuracy of fit were obtained from the combination of Orbach, direct and Raman relaxations: U_{eff} = 8.4 K, $\tau_0 = 2.4 \times 10^{-6}$ s, C = 0.01 K^{-9} s^{-1}, n = 9 (fixed), and aB^4 = 2800 K^{-1} s^{-1} (Table 4, Fig. 4c, red curve).

As an alternative to the well-known relaxation eqn (3), Long and co-workers[19] have proposed a model that considers the relaxation of magnetization through the α-th phonon mode. By following the protocol in their report and incorporating experimentally obtained data on three phonon modes along with their vibronic couplings for compound **2** (Table 5), the phonon contribution to overall relaxation of magnetization can be expressed as linear dependence of temperature

$$\frac{1}{\tau_{phonon}} = \sum_{\alpha}\left(\frac{{V_\alpha}^2}{\hbar}\frac{\Delta_\alpha(2n_\alpha+1)}{({\Delta_\alpha}^2+(\hbar\omega_\alpha)^2)}\right) = 231.64\frac{1}{T} - 66.08 \quad (4)$$

where V_α is the parameter of spin–phonon coupling, Δ_α is the phonon linewidth, n_α is the phonon occupation number, ω_α is the phonon frequency, and $\hbar$ is Planck's constant. Both Δ_α and n_α are dependent on both temperature and frequency of the α-th phonon ω_α. The combination of the phonon, Orbach and direct relaxations resulted in the successful reproduction of the $\ln\tau$ *vs.* $1/T$ dependence (Fig. 4c, blue dashed curve) with fitted parameters given in Table 4.

In light of the observed magnetic properties of the four ionic and complex compounds **1–4**, the question arises whether the SRM originates from the hexacoordinated cations $[Co(L^n)_2]^{2+}$ or the tetracoordinated anions $[Co(NCY)_4]^{2-}$. Based on the numerous previous reports of HS hexacoordinated Co(II) SIMs, we can anticipate that the observed SRM likely originates from the $[Co(L^n)_2]^{2+}$ complex cations.[5] However, the contribution of $[Co(NCY)_4]^{2-}$ cannot be ruled out. Shao and co-workers[10b] reported two spin-crossover active compounds, $[Co(Brphterpy)_2][BPh_4]$ and $[Co(Brphterpy)_2][Co(NCS)_4]\cdot 2MeCN$ (where Brphterpy = 4′-(4-(pyridin-4-yl)phenyl)-[2,2′:6′,2″]terpyridine), in which they also investigated SRM at low temperatures. Both compounds contain the LS complex cation $[Co(Brphterpy)_2]^{2+}$ (S = 1/2). While there was no SRM in $[Co(Brphterpy)_2][BPh_4]$ even under an applied DC field, the latter compound with the LS $[Co(Brphterpy)_2]^{2+}$ cation and HS $[Co(NCS)_4]^{2-}$ anion did show field-induced SRM. Furthermore, Chen and co-workers[14] also observed field-induced SRM in $(Ph_4P)_2[Co(NCO)_4]$ and $(Ph_4P)_2[Co(NCS)_4]$ complex salts, which contain diamagnetic counter cations Ph_4P^+. Thus, these two reports suggest that SRM in compounds **1–4** might originate from the synergistic effects of both the hexacoordinated complex cations and the tetracoordinated anions.

Table 4 Relaxation parameters for compounds **2** and **3** obtained from τ *vs.* B dependencies at 2 K

	Compound **2**	Compound **3**
Raman	d = 71.90 ± 15.75 s^{-1} K^{-9}	d = 380.25 ± 23.23 s^{-1} K^{-9}
	e = 18.27 ± 10.5 T^{-2}	e = 25.70 ± 6.8 T^{-2}
	f = 106.08 ± 57.99 T^{-2}	f = 68.73 ± 18.07 T^{-2}
	n = 9 (fixed)	n = 9 (fixed)
Direct	A = (96 822.44 ± 16 589.62) s^{-1} T^{-4} K^{-1}	A = (232 020.72 ± 17 858.27) s^{-1} T^{-4} K^{-1}
	m = 4 (fixed)	m = 4 (fixed)
R^2	0.97451	0.99113

Summary

In this paper, we reported on the synthesis, crystal structures, static magnetic properties and field-induced single-molecule magnet behaviour of four structurally similar Co(II) coordination compounds, consisting of hexacoordinate complex cations and tetracoordinate anions. The structural analysis unveiled the distorted octahedral shape of coordination polyhedra, where the Co(II) central atom is coordinated with two

Table 5 Relaxation parameters for compound **2** at B_{DC} = 0.3 T

Model	U_{eff}/k_B/K	τ_0/s	C/K^{-n} s^{-1}; n	aB^m/K^{-1} s^{-1}	R^2
Orbach for 4.5–5.5 K	12.4(4) (7.2 cm^{-1})	$7.2(6) \times 10^{-7}$	—	—	0.99521
Orbach & Raman & direct	8(1) (5.6 cm^{-1})	$2.4(6) \times 10^{-6}$	$1.0(0.3) \times 10^{-2}$; 9 (fixed)	2800(1503)	0.99377
Orbach & direct & spin–phonon coupling	10.3(9) (7.2 cm^{-1})	$1.6(3) \times 10^{-6}$	—	4116(815)	0.9939

tridentate derivatives of 2,6-bis(benzimidazole-1-yl)pyridine, decorated by *n*-hexyl, *n*-octyl and *n*-dodecyl substituents. Within the complex anions, the Co(II) metal centre is coordinated with four cyanate or isothiocyanate ligand anions, forming moderately distorted tetrahedra. The comprehensive analysis of the electronic structure and magnetic properties of the reported compounds allowed us to evaluate the axial D parameters, separately for tetrahedral and octahedral coordination sites. FIRMS measurements identified magnetic absorption around the expected value for the ZFS in the presence of phonons, which have an impact on the slow relaxation of magnetisation. AC susceptibility investigations revealed field-induced single-molecule magnet behaviour in all four complexes. However, only one compound exhibited relaxation times accessible for detection with conventional magnetometers. Thorough analysis of the temperature dependence of relaxation times suggests that the slow relaxation of magnetization in this compound is governed by a combination of several relaxation processes, with the spin–phonon coupling contribution being a potential factor that cannot be ruled out. The other three compounds showed very fast relaxation of magnetisation, which was not possible to monitor by conventional dynamic magnetic measurements.

Author contributions

J. J.: synthesis, formal analysis, data curation, writing – original draft, and writing – review & editing; V. T. S.: data curation, investigation, visualization, writing – original draft, and writing – review and editing; J. P.: theoretical investigation, visualization, writing – original draft, and writing – review and editing; J. M.: data curation, investigation, visualization, writing – original draft, and writing – review and editing; I. N.: data curation, investigation, visualization, writing – original draft, and writing – review and editing; M. C.-L.: data curation and writing – review and editing; K. S. K.: data curation and writing – review and editing; M. R.: conceptualization, resources, and writing – review & editing; E. Č.: data curation and writing – review and editing; I. Š.: conceptualization, funding acquisition, resources, supervision, data curation, writing – original draft, visualization, and writing – review & editing.

Data availability

The crystallographic information files (cifs) are available in the CCDC database under the reference numbers 2352529–2352532.† All other data can be made available upon reasonable request. We are not able to store it in a public database due to data size considerations.

Conflicts of interest

There are no conflicts to declare.

Acknowledgements

The authors gratefully acknowledge the financial support of "Large Project for Excellent Researchers" (Nr. 09I03-03-V03-00029). Slovak grant agencies (APVV-19-0087, APVV-22-0172, DS-FR-22-0010 and VEGA 1/0029/22) are acknowledged for the financial support. J. J., I. N. V. T. S. and I. Š. acknowledge the financial support from the Grant Agency of the Czech Republic Grant No. 22-23760S. J. P. is grateful to the HPC center at the Slovak University of Technology in Bratislava, which is a part of the Slovak Infrastructure of High Performance Computing [SIVVP project, ITMS code 26230120002, funded by the European region development funds (ERDF)]. I. N. acknowledges the financial support from the institutional sources of the Department of Inorganic Chemistry, Palacký University Olomouc, Czech Republic. Financial support from the Spanish MCIN (Grant PID2020-117264GB-I00 funded by MCIN/AEI/10.13039/501100011033 and Unidad de Excelencia María de Maeztu CEX2019-000919-M) and the Generalitat Valenciana (PROMETEO program) is acknowledged. We all thank J. M. Martínez-Agudo and G. Agustí for magnetic measurements.

References

1 (*a*) D. Gatteschi, R. Sessoli and J. Villain, *Molecular Nanomagnets*, Oxford University Press, 2006; (*b*) S. Gao, *Molecular Nanomagnets and Related Phenomena*, Springer-Verlag, Berlin-Heidelberg, 2015, vol. 164; (*c*) J. Tang and P. Zhang, *Lanthanide Single Molecule Magnets*, 2015, pp. 1–211; (*d*) S. T. Liddle and J. Van Slageren, Improving f-element single molecule magnets, *Chem. Soc. Rev.*, 2015, **44**, 6655–6669; (*e*) A. Zabala-Lekuona, J. M. Seco and E. Colacio, Single-Molecule Magnets: From Mn12-ac to dysprosium metallocenes, a travel in time, *Coord. Chem. Rev.*, 2021, **441**, 213984; (*f*) Z. Zhu and J. Tang, Covalent organic framework photocatalysts: structures and applications, *Chem. Soc. Rev.*, 2022, **51**, 9469–9481.

2 (*a*) E. Coronado, Molecular magnetism: from chemical design to spin control in molecules, materials and devices, *Nat. Rev. Mater.*, 2019, **5**, 87–104; (*b*) J. J. Dugay, M. Aarts, M. Gimenez-Marqués, T. Kozlova, H. W. Zandbergen, E. Coronado and H. S. J. Van Der Zant, Phase Transitions in Spin-Crossover Thin Films Probed by Graphene Transport Measurements, *Nano Lett.*, 2017, **17**, 186–193; (*c*) M. Urdampilleta, S. Klyatskaya, J. P. Cleuziou, M. Ruben and W. Wernsdorfer, Supramolecular spin valves, *Nat. Mater.*, 2011, **10**, 502–506.

3 A. Ardavan, O. Rival, J. J. L. Morton, S. J. Blundell, A. M. Tyryshkin, G. A. Timco and R. E. P. Winpenny, Will Spin-Relaxation Times in Molecular Magnets Permit Quantum Information Processing?, *Phys. Rev. Lett.*, 2007, **98**, 057201.

4 D. Tanaka, N. Aketa, H. Tanaka, S. Horike, M. Fukumori, T. Tamaki, T. Inose, T. Akai, H. Toyama, O. Sakata, H. Tajiri

and T. Ogawa, Facile preparation of hybrid thin films composed of spin-crossover nanoparticles and carbon nanotubes for electrical memory devices, *Dalton Trans.*, 2019, **48**, 7074–7079.

5 (*a*) J. M. Frost, K. L. M. Harriman and M. Murugesu, The rise of 3-d single-ion magnets in molecular magnetism: towards materials from molecules?, *Chem. Sci.*, 2016, **7**, 2470–2491; (*b*) J. Juráková and I. Šalitroš, Co(II) single-ion magnets: synthesis, structure, and magnetic properties, *Monatsh. Chem.*, 2022, **153**, 1001–1036.

6 (*a*) R. Boča, Zero-field splitting in metal complexes, *Coord. Chem. Rev.*, 2004, **248**, 757–815; (*b*) T. Wu, Y.-Q. Zhai, Y.-F. Deng, W.-P. Chen, T. Zhang and Y.-Z. Zheng, Correlating magnetic anisotropy with the subtle coordination geometry variation of a series of cobalt(II)-sulfonamide complexes, *Dalton Trans.*, 2019, **48**, 15419–15426; (*c*) Y.-Q. Zhai, Y.-F. Deng and Y.-Z. Zheng, Pseudotetrahedral cobalt(II) complexes with PNP-ligands showing uniaxial magnetic anisotropy, *Dalton Trans.*, 2018, **47**, 8874–8878; (*d*) Y.-F. Deng, Z. Wang, Z.-W. Ouyang, B. Yin, Z. Zheng and Y.-Z. Zheng, Large Easy-Plane Magnetic Anisotropy in a Three-Coordinate Cobalt(II) Complex $[Li(THF)_4][Co(NPh_2)_3]$, *Chem. – Eur. J.*, 2016, **22**, 14821–14825.

7 (*a*) J. Juráková, J. D. Midlíková, J. Hrubý, A. Kliuikov, V. T. Santana, J. Pavlik, J. Moncoľ, E. Čižmár, M. Orlita, I. Mohelský, P. Neugebauer, D. Gentili, M. Cavallini and I. Šalitroš, Pentacoordinate cobalt(II) single ion magnets with pendant alkyl chains: shall we go for chloride or bromide?, *Inorg. Chem. Front.*, 2022, **9**, 1179–1194; (*b*) J. Juráková, O. F. Fellner, S. Schlittenhardt, Š. Vavrečková, I. Nemec, R. Herchel, E. Čižmár, V. T. Santana, M. Orlita, D. Gentili, G. Ruani, M. Cavallini, P. Neugebauer, M. Ruben and I. Šalitroš, Neutral cobalt(II)-bis(benzimidazole)pyridine field-induced single-ion magnets for surface deposition, *Inorg. Chem. Front.*, 2023, **10**, 5406–5419; (*c*) N. Malinová, J. Juráková, B. Brachňaková, J. D. Midlíková, E. Čižmár, V. T. Santana, R. Herchel, M. Orlita, I. Mohelský, J. Moncol, P. Neugebauer and I. Šalitroš, Magnetization Slow Dynamics in Mononuclear Co(II) Field-Induced Single-Molecule Magnet, *Cryst. Growth Des.*, 2023, **23**, 2430–2441.

8 (*a*) B. Brachňaková, S. Matejová, J. Moncol, R. Herchel, J. Pavlik, E. Moreno-Pineda, M. Ruben and I. Šalitroš, Stereochemistry of coordination polyhedra vs. single ion magnetism in penta- and hexacoordinated Co(II) complexes with tridentate rigid ligands, *Dalton Trans.*, 2020, **49**, 1249–1264; (*b*) A. K. Mondal, T. Goswami, A. Misra and S. Konar, Probing the Effects of Ligand Field and Coordination Geometry on Magnetic Anisotropy of Pentacoordinate Cobalt(II) Single-Ion Magnets, *Inorg. Chem.*, 2017, **56**, 6870–6878.

9 S. Ghosh, S. Kamilya, M. Das, S. Mehta, M. E. Boulon, I. Nemec, M. Rouzières, R. Herchel and A. Mondal, Impact of Counteranion on Reversible Spin-State Switching in a Series of Cobalt(II) Complexes Containing a Redox-Active Ethylenedioxythiophene-Based Terpyridine Ligand, *Inorg. Chem.*, 2020, **59**, 7067–7081.

10 (*a*) K. Choroba, J. Palion-Gazda, B. Machura, A. Bieńko, D. Wojtala, D. Bieńko, C. Rajnák, R. Boča, A. Ozarowski and M. Ozerov, Large Magnetic Anisotropy in Mono- and Binuclear cobalt(II) Complexes: The Role of the Distortion of the Coordination Sphere in Validity of the Spin-Hamiltonian Formalism, *Inorg. Chem.*, 2024, **63**, 1068–1082; (*b*) D. Shao, L. D. Deng, L. Shi, D. Q. Wu, X. Q. Wei, S. R. Yang and X. Y. Wang, Slow Magnetic Relaxation and Spin-Crossover Behavior in a Bicomponent Ion-Pair Cobalt (II) Complex, *Eur. J. Inorg. Chem.*, 2017, **2017**, 3862–3867; (*c*) Y. Zhang, K. L. M. Harriman, G. Brunet, A. Pialat, B. Gabidullin and M. Murugesu, Reversible Redox, Spin Crossover, and Superexchange Coupling in 3d Transition-Metal Complexes of Bis-azinyl Analogues of 2,2′: 6′,2″-Terpyridine, *Eur. J. Inorg. Chem.*, 2018, 1212–1223; (*d*) A. Galet, A. B. Gaspar, M. C. Muñoz and J. A. Real, Influence of the Counterion and the Solvent Molecules in the Spin Crossover System $[Co(4\text{-terpyridone})_2]Xp.nH_2O$, *Inorg. Chem.*, 2006, **45**, 4413–4422; (*e*) J. Palion-Gazda, B. Machura, R. Kruszynski, T. Grancha, N. Moliner, F. Lloret and M. Julve, Spin Crossover in Double Salts Containing Six- and Four-Coordinate Cobalt(II) Ions, *Inorg. Chem.*, 2017, **56**, 6281–6296; (*f*) S. S. Massoud, M. Dubin, A. E. Guilbeau, M. Spell, R. Vicente, P. Wilfling, R. C. Fischer and F. A. Mautner, Azido- and thiocyanato-cobalt(II) complexes based pyrazole ligands, *Polyhedron*, 2014, **78**, 135–140.

11 M. G. B. Drew, C. J. Harding, V. McKee, G. G. Morgan and J. Nelson, Geometric control of manganese redox state, *J. Chem. Soc., Chem. Commun.*, 1995, 1035–1038.

12 (*a*) S. Alvarez, D. Avnir, M. Llunell and M. Pinsky, Continuous symmetry maps and shape classification. The case of six-coordinated metal compounds, *New J. Chem.*, 2002, **26**, 996–1009; (*b*) M. Llunell, D. Casanova, J. Cirera, P. Alemany and S. Alvarez, *SHAPE version 2.0*, 2010, Universitat de Barcelona, Barcelona.

13 L. Banci, A. Bencini, C. Benelli, D. Gatteschi and C. Zanchini, *Structures versus Special Properties*, 1982, pp. 37–86.

14 S.-Y. Chen, W. Lv, H.-H. Cui, L. Chen, Y.-Q. Zhang, X.-T. Chen, Z. Wang and Z.-W. Ouyang, H Yan, and Zi-Ling Xue, Magnetic anisotropies and slow magnetic relaxation of three tetrahedral tetrakis(pseudohalido)–cobalt(II) complexes, *New J. Chem.*, 2021, **45**, 16852–16861 and the references therein.

15 (*a*) A. T. Hand, B. D. Watson-Sanders and Z. L. Xue, *Dalton Trans.*, 2024, **53**, 4390–4405; (*b*) A. L. Nagelski, M. Ozerov, M. S. Fataftah, J. Krzystek, S. M. Greer, P. L. Holland and J. Telser, Spectroscopic techniques to probe magnetic anisotropy and spin–phonon coupling in metal complexes, *Inorg. Chem.*, 2024, **63**, 4511–4526; (*c*) J. Krzystek and J. Telser, Measuring giant anisotropy in paramagnetic transition metal complexes with relevance to single-ion magnetism, *Dalton Trans.*, 2016, **45**, 16751–16763; (*d*) J. J. Liu, Y. S. Meng, I. Hlavička, M. Orlita, S. Da Jiang, B. W. Wang

and S. Gao, Determination of zero-field splitting in Co2+ halide complexes with magnetic and far-IR measurements, *Dalton Trans.*, 2017, **46**, 7408–7411; (*e*) D. H. Moseley, Z. Liu, A. N. Bone, S. E. Stavretis, S. K. Singh, M. Atanasov, Z. Lu, M. Ozerov, K. Thirunavukkuarasu, Y. Cheng, L. L. Daemen, D. Lubert-Perquel, D. Smirnov, F. Neese, A. J. Ramirez-Cuesta, S. Hill, K. R. Dunbar and Z. L. Xue, Spectroscopic Studies of the Magnetic Excitation and Spin-Phonon Couplings in a Single-Molecule Magnet, *Inorg. Chem.*, 2022, **61**, 17123–17136; (*f*) J. Nehrkorn, J. Telser, K. Holldack, S. Stoll and A. Schnegg, Simulating Frequency-Domain Electron Paramagnetic Resonance: Bridging the Gap between Experiment and Magnetic Parameters for High-Spin Transition-Metal Ion Complexes, *J. Phys. Chem. B*, 2015, **119**, 13816–13824; (*g*) E. Ferentinos, D. Tzeli, S. Sottini, E. J. J. Groenen, M. Ozerov, G. Poneti, K. Kaniewska-Laskowska, J. Krzystek and P. Kyritsis, Magnetic anisotropy and structural flexibility in the field-induced single ion magnets $[Co\{(OPPh_2)(EPPh_2)N\}_2]$, E=S, Se, explored by experimental and computational methods, *Dalton Trans.*, 2023, **52**, 2036–2050.

16 D. H. Moseley, S. E. Stavretis, K. Thirunavukkuarasu, M. Ozerov, Y. Cheng, L. L. Daemen, J. Ludwig, Z. Lu, D. Smirnov, C. M. Brown, A. Pandey, A. J. Ramirez-Cuesta, A. C. Lamb, M. Atanasov, E. Bill, F. Neese and Z. L. Xue, Spin–phonon couplings in transition metal complexes with slow magnetic relaxation, *Nat. Commun.*, 2018, **9**, 1–11.

17 A. Abragam and B. Bleaney, *Electron paramagnetic resonance of transition ions*, Clarendon press, Oxford, 1970, vol. 911.

18 S. Nain, M. Kumar and M. E. Ali, The impact of spin-vibrational coupling on magnetic relaxation of a Co(II) single-molecule magnet, *Phys. Chem. Chem. Phys.*, 2023, **25**, 14848–14861.

19 P. C. Bunting, M. Atanasov, E. Damgaard-Møller, M. Perfetti, I. Crassee, M. Orlita, J. Overgaard, J. van Slageren, F. Neese and J. R. Long, A linear cobalt(II) complex with maximal orbital angular momentum from a non-Aufbau ground state, *Science*, 2018, **362**, 1378.